Article

Rainfall-Induced Shallow Landslide Recognition and Transferability Using Object-Based Image Analysis in Brazil

Helen Cristina Dias [1,*] , Daniel Hölbling [2] and Carlos Henrique Grohmann [1]

1 Institute of Energy and Environment, University of São Paulo (IEE-USP), Av. Prof. Luciano Gualberto, 1289, Cidade Universitária, São Paulo 05508-900, Brazil

2 Department of Geoinformatics—Z_GIS, University of Salzburg, Schillerstraße 30, 5020 Salzburg, Austria

* Correspondence: helendias71@gmail.com

Abstract: Landslides are among the most frequent hazards in Latin America and the world. In Brazil, they occur every year and cause economic and social loss. Landslide inventories are essential for assessing susceptibility, vulnerability, and risk. Over the decades, a variety of mapping approaches have been employed for the detection of landslides using Earth observation (EO) data. Object-based image analysis (OBIA) is a widely recognized method for mapping landslides and other morphological features. In Brazil, despite the high frequency of landslides, methods for inventory construction are poorly developed. The aim of this study is to semi-automatically recognize shallow landslides in Itaóca (Brazil) and evaluate the transferability of the approach within different areas in Brazil. RapidEye satellite images (5 m) and the derived normalized difference vegetation index (NDVI), as well as a digital elevation model (DEM) (12.5 m) and morphological data, were integrated into the classification. The results show that the method is suitable for the recognition of this type of hazard in Brazil. The overall accuracy was 89%. The main challenges were the identification of small landslides and the exact delineation of scars. The findings validate the applicability of the approach in Brazil, although additional adjustments to the primary rule set might lead to better results.

Keywords: inventory; mass movement; semi-automated mapping; expert knowledge integration; remote sensing; Serra do Mar

1. Introduction

Landslides are one of the most common and destructive natural hazards worldwide and were responsible for 500 deaths and an economic loss of USD 500 million in 2021 [1]. Latin America is highly affected by landslides, and it is considered a prone area due to local conditions (e.g., geological, geomorphological, and meteorological conditions) [2]. The region is profoundly conditioned by its colonial past, and society suffers from poverty, environmental degradation, and the absence of governmental strategic policies for territorial management to address disasters [2].

Rainfall-triggered fatal landslide events occur frequently in Brazil, resulting in many economic and social problems [3–5]. According to Alvalá et al. [6], out of every 100 inhabitants, nine resided in areas vulnerable to disasters within the country. The presence of such an exposed population is attributed to the absence of adequate urban planning and a lack of a consistent policy for hazards and disaster management [7]. Despite the high frequency of mass movement events and the population at risk, landslide inventories have been poorly developed in Brazil [8,9]. Inventory maps document all landslide features triggered in a location and are essential for risk and susceptibility studies and territorial planning and management [10]. After a high-magnitude landslide event in 2011 [11,12], the Brazilian Federal Government established the *National Policy on Protection and Civil Defense*, with law No. 12,608 of 10 April 2012, to avoid possible new landslide occurrences, and two of the main guidelines are directly related to landslide inventory construction (Source:

http://www.planalto.gov.br/ccivil_03/_Ato2011-2014/2012/Lei/L12608.htm, accessed on 14 September 2023). In recent years, there has been an increasing amount of literature on mapping event-triggered landslides in Brazil using various methods (e.g., manual, semi-automated, and automated) [13–20]. In general, these studies have concentrated on recognizing landslide features and characterizing individual mass movement events, without a primary focus on assessing the transferability of these approaches within the Brazilian national territory. Object-based image analysis (OBIA) is a well-established method for mapping landslides and geomorphological features [21–25], with significant potential for the detection of landslides in satellite imagery [21,23,24,26]. Considerable progress has been made in applying the OBIA method to landslide analysis in recent years. Numerous studies have adopted diverse semi-automated approaches, primarily utilizing optical satellite images and DEM data [26]. For instance, semi-automated methods have been combined with machine learning algorithms [27,28], merging optical and DEM data to automatically detect and distinguish various landslide types [22,25,29,30]. These studies have also involved the use of open source tools and software [31,32], time series analysis with optical satellite data [33], and comparisons between OBIA results and visual image interpretation [23].

Although several studies have demonstrated the applicability of OBIA for landslide mapping in various environments, its application for landslide mapping in tropical environments in Brazil is still incipient. Brazilian studies which applied OBIA, for example, focused on urban infrastructure, coral reefs, gullies, and vegetation pattern mapping, and not on natural hazards [34–38]. This method considerably simulates human cognition and enables the transfer of existing knowledge into machine-executable rule sets [27]. OBIA involves two main steps: image segmentation and classification [39–41]. Segmentation is the division of an image into objects [39]. Relatively homogeneous pixels are grouped into meaningful objects using varied information [40]. This is the initial and most important procedure because the accuracy of the extracted objects and further classification depends on the quality of the segmentation [42]. During classification, several characteristics can be used to describe and classify objects, such as spectral values, spatial, textural, and morphological, as well as relationships between objects, proximity, and connectivity [40]. The input data are a crucial aspect to consider, as selecting the appropriate combination of layers and parameters directly impacts the recognition of features. The selection process must take into account the conditions influencing shallow landslide occurrence (e.g., slope). Data resolution is also of great importance. For example, in the case of shallow landslides, the size of the features varies significantly, and only may be useful for the detection and classification of high- or very-high-resolution images. Landslides are complex geomorphological features that should be treated as objects when mapping them. By using OBIA, landslides can be considered clusters of pixels instead of individual pixels without spatial correlation [43]. The method allows for the creation of rule sets that are ideally transferable to other study sites with similar environmental characteristics, requiring only minor adjustments in thresholds [33]. This is very helpful in Brazil since the country has a continental dimension (8,515,767.049 km^2) and mass movements occur frequently in different regions. Moreover, utilizing a pre-developed rule set for a recent event can enhance the generation of new inventories, thereby contributing to effective territorial management. Thus, the aim of this study was to recognize shallow landslides in Itaóca (Brazil) triggered in January 2014 and evaluate the transferability of the approach within different areas in Brazil.

2. Study Area

The study area is the Itaóca municipality, located in the south of the state of São Paulo, southeastern Brazil (Figure 1). Itaóca is a small municipality in the Ribeira Valley with an approximate population of 3200 in a total area of 183 km^2 [44]. The site is covered by the Atlantic Forest. It is characterized by elevations up to 1100 m.a.s.l., steep slopes, and a temperature range between 11 °C and 30 °C [45]; the climate type is Humid subtropical (Cfa), characterized by hot summers and frequent thunderstorms. The geology and

pedology consist of Archean-Proterozoic igneous and metamorphic rocks, predominantly granite [46,47], and cambisols, leptsols, acrisols, and gleysols [48].

Rainfall-triggered mass movements occurred in Itaóca on 12 January 2014. As a consequence of the numerous shallow landslides and debris flows, the local infrastructure (e.g., roads, bridges, and energy supply) and 100 houses were destroyed, and 25 people died [49,50]. The study site covers an area of 51 km^2 and includes three watersheds: Guarda-mão, Gurutuba, and Palmital. According to Dias et al. [51], the area has a medium to high susceptibility to debris flows. Debris flows in Brazil are mostly triggered by shallow landslides, and local geomorphological conditions favor the transportation of high volumes of sediments [51].
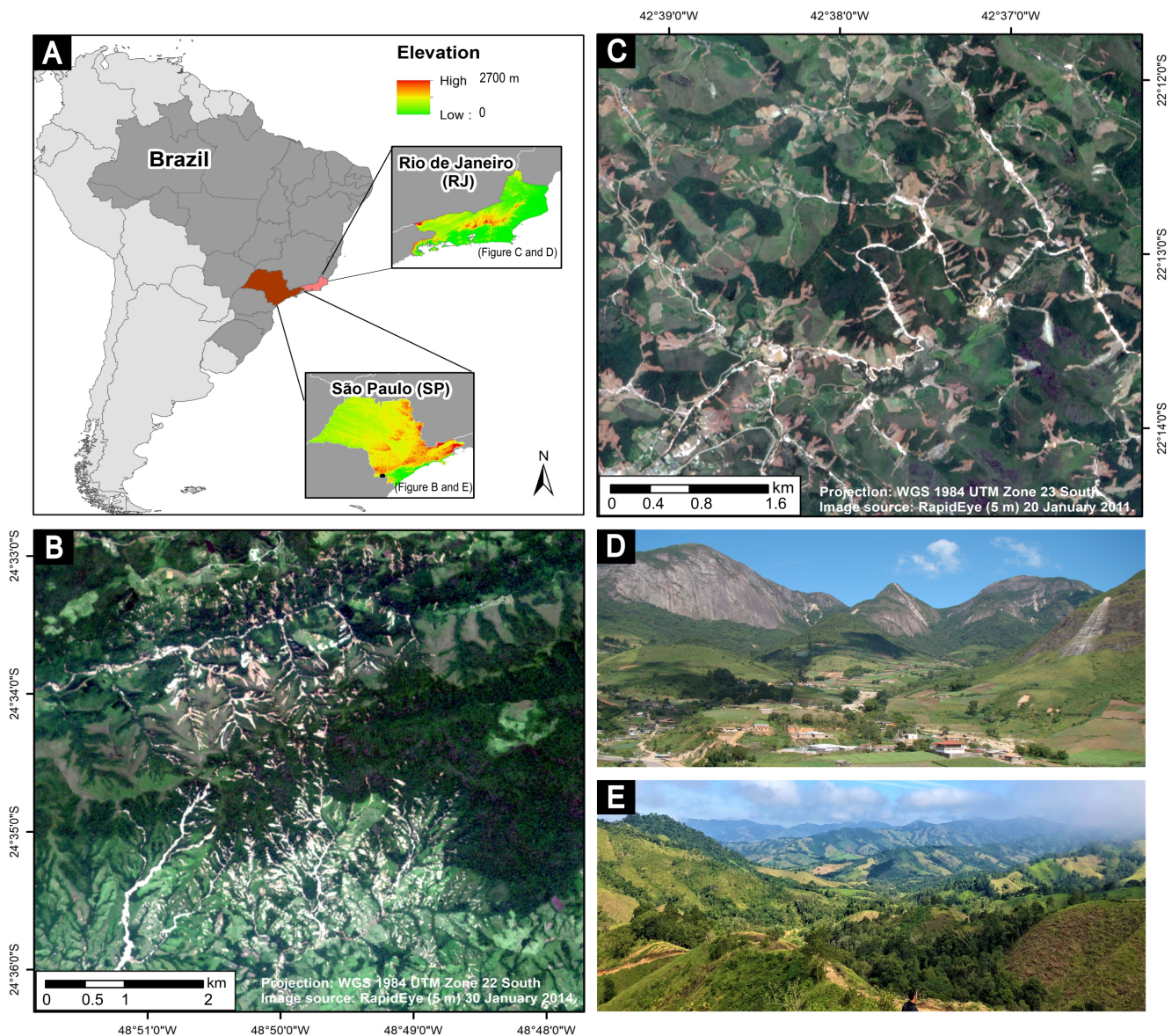

Figure 1. (**A**) Location of the study areas in Brazil; (**B**) Itaóca in 2014 after the mass movement a high-magnitude event; (**C**) Nova Friburgo in 2011 after the mass movement high-magnitude event; (**D**) Mountains in Nova Friburgo. Photograph: M.F. Gramani; (**E**) Mountains in Itaóca. Photograph: V.C. Dias.

The second study site is Nova Friburgo (Figure 1), located in the mountainous region of Rio de Janeiro state, southeastern Brazil. Nova Friburgo is a municipality with an approximate population of 192,000 in a total area of 936 km^2 [44]. The site was selected to

evaluate the transferability of the landslide mapping approach. The area is in the Serra dos Orgãos geomorphological unit and is characterized by elevations of up to 2000 m.a.s.l. and the Atlantic Forest [52]. The geology mainly consists of igneous and metamorphic rocks (e.g., granites, gabbros, and gneisses) [53]. In January 2011, Nova Friburgo was affected by a high-magnitude mass movement event, which is considered the most destructive event in Brazilian history [11]. Extreme rainfall triggered many landslides, resulting in more than 1500 deaths, and damage to buildings and infrastructure [12].

3. Materials and Methods

3.1. Data

The satellite images used in this study were RapidEye Analytic Ortho Tile multispectral images (5 m spatial resolution), a radiometric resolution of 16 bit, and five spectral bands (blue, red, green, red edge, and near-infrared (NIR)) [54]. The normalized difference vegetation index (NDVI) was computed by assessing the difference in reflectance in the NIR and red bands. The NDVI has been widely used for vegetation monitoring and assessment and is commonly applied in landslide studies [15,55,56]. In Itaóca (SP), the 1:10,000 scale drainage network provided by the Geographic and Cartographic Institute of the State of São Paulo (IGC-SP) was utilized, while in Nova Friburgo (RJ), a drainage network at a 1:25,000 scale from the National Water and Basic Sanitation Agency (ANA) was employed. Additional data, such as slope, curvature, and flow accumulation, were derived from the ALOS PALSAR DEM with a resolution of 12.5 m [57]. An overview of the data is presented in Table 1.

Table 1. Overview of the datasets.

Dataset	Source	Scale/Resolution	Description
Satellite imagery	RapidEye	5 m	Five multispectral bands (blue, red, green, red edge, and near-infrared). Acquisition dates: 30 January 2014 (SP); 20 January 2011 (RJ)
DEM	ALOS	12.5 m	Parameters used: slope, curvature, flow accumulation. Format: raster.
Drainage network	IGC-SP	1:10,000	Geographic and Cartographic Institute of the State of São Paulo. Format: vector.
	ANA	1:25,000	National Water and Basic Sanitation Agency. Format: vector.

3.2. Object-Based Mass Movement Mapping

For semi-automated shallow landslide mapping, an OBIA method was employed, utilizing the eCognition 10.0 (Trimble) software. For segmentation, the multiresolution segmentation algorithm was applied. The algorithm consecutively merges adjacent pixels or existing segments based on homogeneity, which is determined through a combination of spectral and shape criterion [58]. The segmentation settings were the same as those used by Dias et al. [30]: scale parameter: 50; shape: 0.3; and compactness: 0.9. These settings were established through a combination of expert knowledge and trial-and-error experimentation, with the goal of generating image objects conducive to the identification of shallow landslides. After segmentation, the objects were classified as shallow landslides based on low NDVI values (near zero). Once the non-vegetated or sparsely vegetated objects were identified with the NDVI, the incorrectly selected drainage channel sectors were removed using the slope angle, and the border to and distance from the drainage network. Upon the completion of the classification workflow, mainly shallow landslides were classified. The main classification parameters are listed in Table 2. The detection and classification of shallow landslides were mainly based on three different metrics: spatial, spectral, and morphological. Shallow landslides result in the exposure of bare ground with little to no vegetation cover; thus, the NDVI was used to identify potential landslide features in the first step, since non-vegetated areas, including bare soil, have low NDVI values near zero [40]. Subsequently, the classification was refined stepwise using the spatial

and morphological characteristics. The metrics selection was based on the classification of Dias et al. [14]. The classification thresholds were determined and tuned based on expert knowledge. A summary of the workflow is shown in Figure 2.

Table 2. Segmentation and classification thresholds used in OBIA.

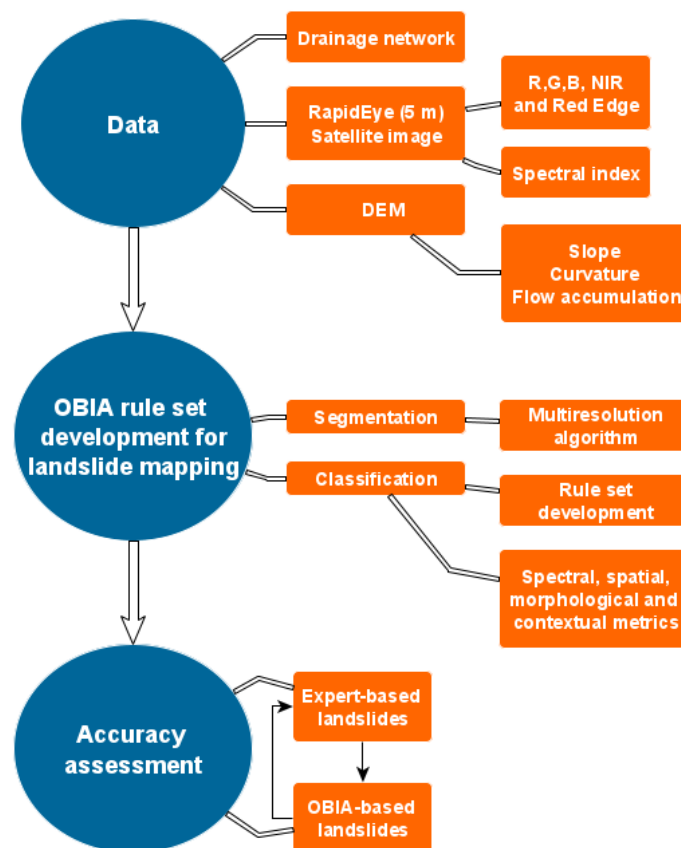| Study Area	Classification Parameters
Itaóca	Mean NDVI $\leq$ 0.32 Mean slope $\geq$ 16 Distance from drainage network $\leq$ 12 m Border to drainage network $\leq$ 0.5 m
Nova Friburgo	Mean NDVI $\leq$ 0.15 Mean slope $\geq$ 12 Distance from drainage network $\leq$ 12 m Border to drainage network $\leq$ 0.5 m

Figure 2. Overview of the processing steps followed in this study.

The workflow was developed for Itaóca and was subsequently tested in Nova Friburgo, whereby only minor adaptations in threshold values were made. This allowed us to evaluate the transferability of the approach and the applicability of the classification parameters among different areas in Brazil. Shallow landslides generally occur under similar conditioning factors in Brazil. Therefore, it was possible to apply the same rule set with only minor adaptations in both study areas. These minor adaptations were necessary due to environmental and urban changes between the study areas.

3.3. Accuracy Assessment

The accuracy of the results was assessed by comparison to a shallow landslide inventory created through expert interpretation [14], taking into account the spatial alignment

between the reference dataset and the new semi-automated classification. The accuracy was assessed by true positives (*TP*), false positives (*FP*), true negatives (*TN*), and false negatives (*FN*), and the recall (Equation (1)), precision (Equation (2)), overall accuracy (OA) (Equation (3)), and *F1 Score* (Equation (4)) were calculated. These indices are common for the validation of landslide recognition and mapping results [15,18,25,33]. *TP* represents correctly classified objects, *FP* represents incorrectly classified objects, *TN* represents correctly classified objects as not shallow landslides, and *FN* represents incorrectly classified objects not as shallow landslides. Recall indicates the probability that a given object has been correctly classified as a landslide, and precision indicates the probability that a classified object represents a landslide [59,60].

$$R = \frac{\sum_{i=1}^{n} TP_1}{\sum_{i=1}^{n} (TP_1 + FP_1)} \tag{1}$$

$$P = \frac{\sum_{i=1}^{n} TP_1}{\sum_{i=1}^{n} (TP_1 + FN_1)} \tag{2}$$

$$OA = 100 \times \frac{(TN + TP)}{TN + FP + FN + TP} \tag{3}$$

$$F1 \; Score = 2 \times \frac{P \times R}{P + R} \tag{4}$$

Furthermore, a series of object-by-object spatial accuracy metrics were computed, aiming to determine the spatial and geometrical agreement between the manually mapped landslide polygons (reference inventory) (A_{Rj}) and the landslide polygons recognized by OBIA (A_{Si}) [23,61]. The OBIA classification requires an object-segmentation. These segmented objects were used for the classification of landslide scars. However, the variability of landslides in size and shape makes it challenging to delineate single landslides as single objects; for this reason, the identification of the exact same number of landslides is complex and remains a challenge [62]. The delineation of OBIA objects did not align with the manual landslide delineation; for instance, one manually identified landslide might encompass several smaller OBIA objects. Objects classified as landslides using OBIA were consequently organized into larger polygons through contiguity and proximity-based merging. Five spatial indexes were used to calculate the geometric similarity of the object's delineations: (I) quality rate (*QR*) (Equation (5)); (II) area fit index (*AFI*) (Equation (6)); (III) over-segmentation rate (*OS*) (Equation (7)); (IV) under-segmentation rate (*US*) (Equation (8)); and (V) root mean square (*D*) (Equation (9)). The spatial indexes are based on area proportions, and their values vary from 0 to 1 (excluding AFI). The spatial alignment between the reference and the test dataset is more accurate when the value is nearest to zero [23,61].

$$QR = 1 - \frac{A_{Rj} \cap A_{Si}}{A_{Rj} \cup A_{Si}} \tag{5}$$

$$AFI = \frac{A_{Rj} - A_{Si}}{A_{Rj}} \tag{6}$$

$$OS = 1 - \frac{A_{Rj} \cap A_{Si}}{A_{Rj}} \tag{7}$$

$$US = 1 - \frac{A_{Rj} \cap A_{Si}}{A_{Si}} \tag{8}$$

$$D = \sqrt{\frac{(OS)^2 + (US)^2}{2}} \tag{9}$$

4. Results

4.1. Semi-Automated Object-Based Mapping of Shallow Landslides

The semi-automated object-based classification of shallow landslides is presented in Figure 3. In general, the approach correctly identified the locations with shallow landslides, but the semi-automated classification underestimates the reference. A total area of 2.73 km^2 (1430 polygons after merging) was categorized as shallow landslides, while the reference inventory presented 3.48 km^2 (1723 polygons). The variance between the semi-automatic classification and the reference inventory amounts to approximately 21%. The spatial overlap of the detected landslides and reference mapping was 54% (i.e., 1.88 km^2) (Figure 4).
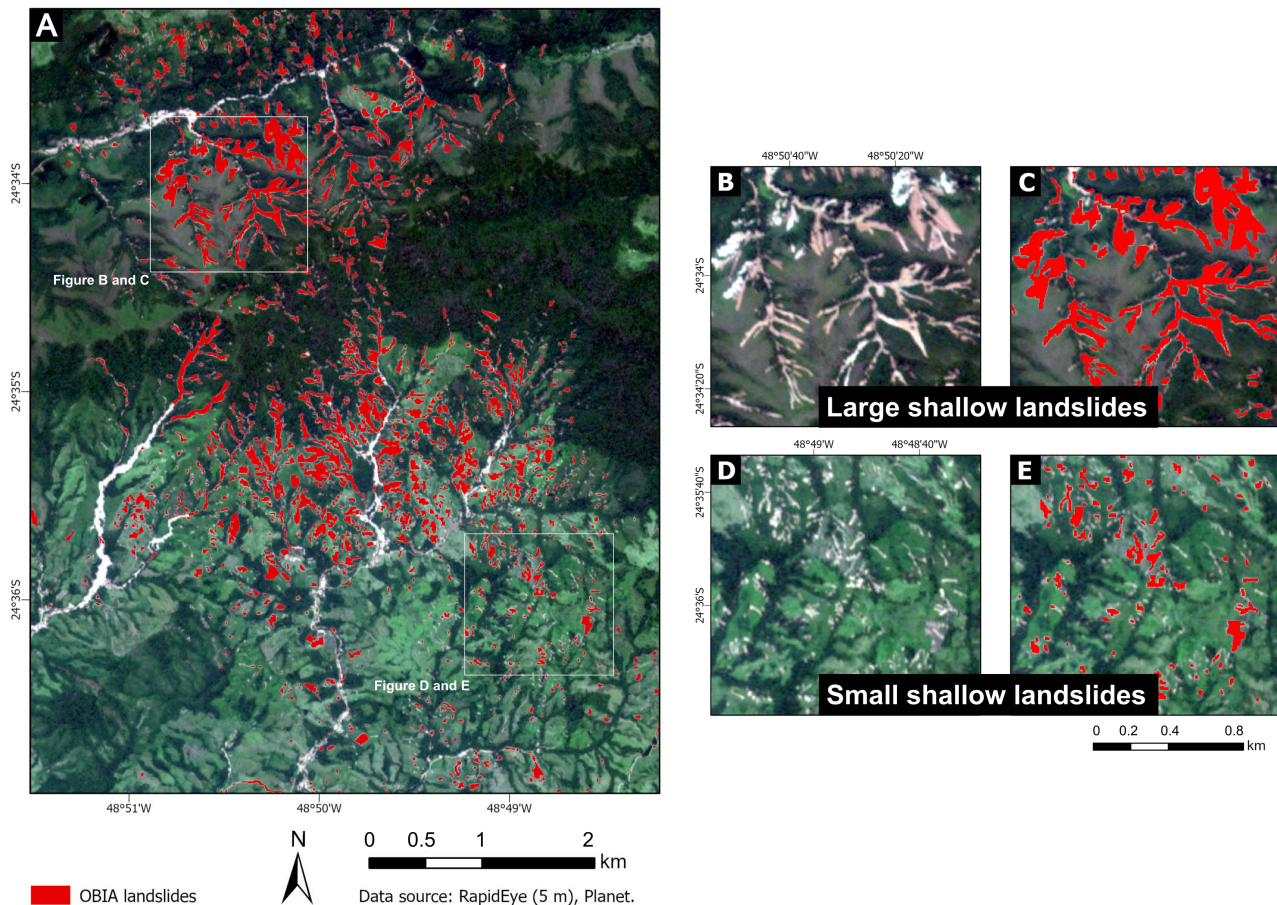

Figure 3. (**A**) Shallow landslide mapping resulting in Itaóca (SP) using OBIA; (**B**) RapidEye image showing large shallow landslides in the northern sector; (**C**) OBIA classification of large shallow landslides in the northern sector; (**D**) RapidEye image showing small shallow landslides in the southern sector; and (**E**) OBIA classification of small shallow landslides in the southern sector.

An *F1 Score* of 88%, precision of 79%, recall of 98%, and *OA* of 89% were achieved. Regarding the spatial accuracy metrics, satisfactory results were achieved, with *QR*: 0.52; *AFI*: 0.33; *OS*: 0.46; *US*: 0.19; and *D*: 0.35. Through the merging of OBIA classification objects, it became feasible to compare the overall count of landslides identified through semi-automated means with the manually conducted mapping. However, several factors limit the comparability in terms of numbers. OBIA failed to detect certain small shallow landslides, and it also erroneously combined adjacent landslides into larger polygons.

Landslide Distribution Analysis

The majority of landslides were concentrated on slopes between 15° and 30°, with elevations between 300 m and 600 m presenting negative values for plan curvature (Figure 5),

and relative low NDVI values (Table 3). Regarding the geology (Figure 5D), shallow landslides are concentrated in the Itaóca batholith zone (Itaóca unit—Barra do Chapéu Granite) [46], which is constituted of quartz monzonite to monzogranite [47]. Landslides are also present in the Lajeado metasedimentary group (Serra da Boa Vista (MPbv), Passa Vinte (MPpv), and Gorotuba (MPg) Formation) in the northern part of the study area, which consists of marble, calc-silicate rocks, phyllite, schist, quartzite, and metabasite [47].
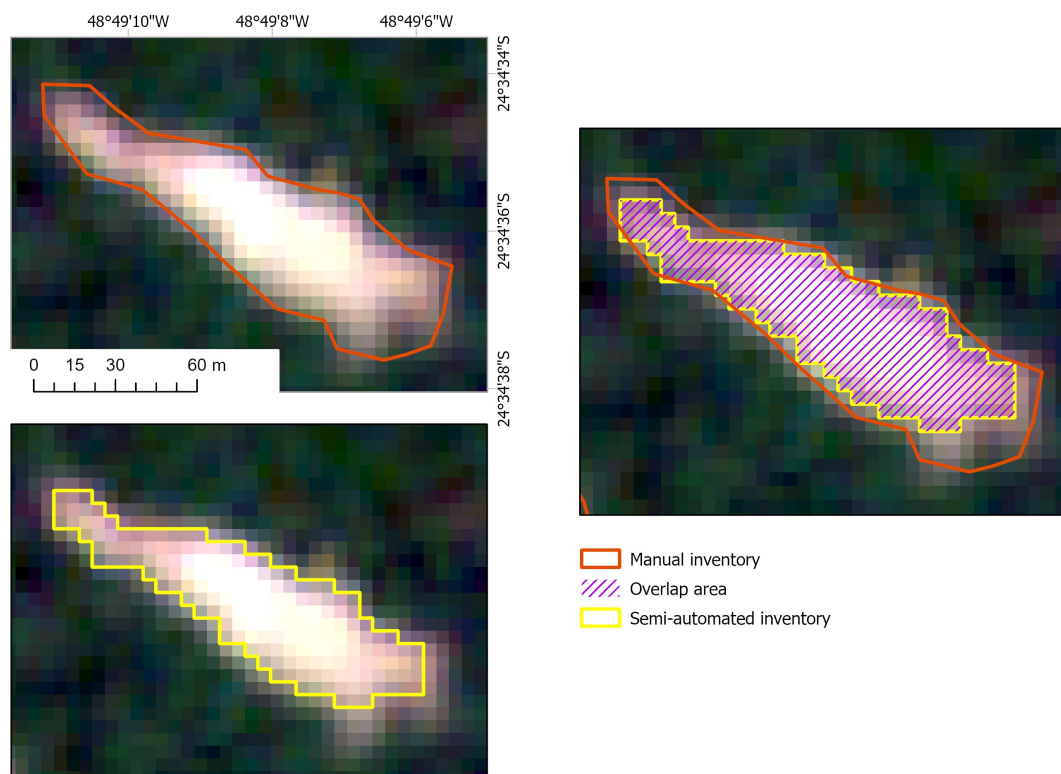

Figure 4. An example of a shallow landslide scar for the comparison of manual and semi-automated mapping and overlap area.

Two different landslide shape patterns were identified based on size (m^2) and format (Figure 3B,D). The north sector has a significant concentration of large and long shallow landslide scars (1.05 km^2) (Figure 3B,C), whereas small-to-medium and rounded scars are concentrated in the central and south sectors (1.6 km^2) (Figure 3D,E). To better understand the different spatial characteristics, the above-described spatial accuracy metrics were calculated separately for each pattern (Table 4). The northern sector shows better accuracy results, especially for the *US* index. A low *US* value (0.25) indicates a high spatial match between the reference inventory and the landslide polygons recognized with OBIA, in other words, there is a high agreement between both delineations. This indicates that large and elongated shallow landslide scars were more easily recognized than small-to-medium and rounded scars.

Table 3. Spectral and morphological characteristics of the shallow landslide inventory produced with OBIA.

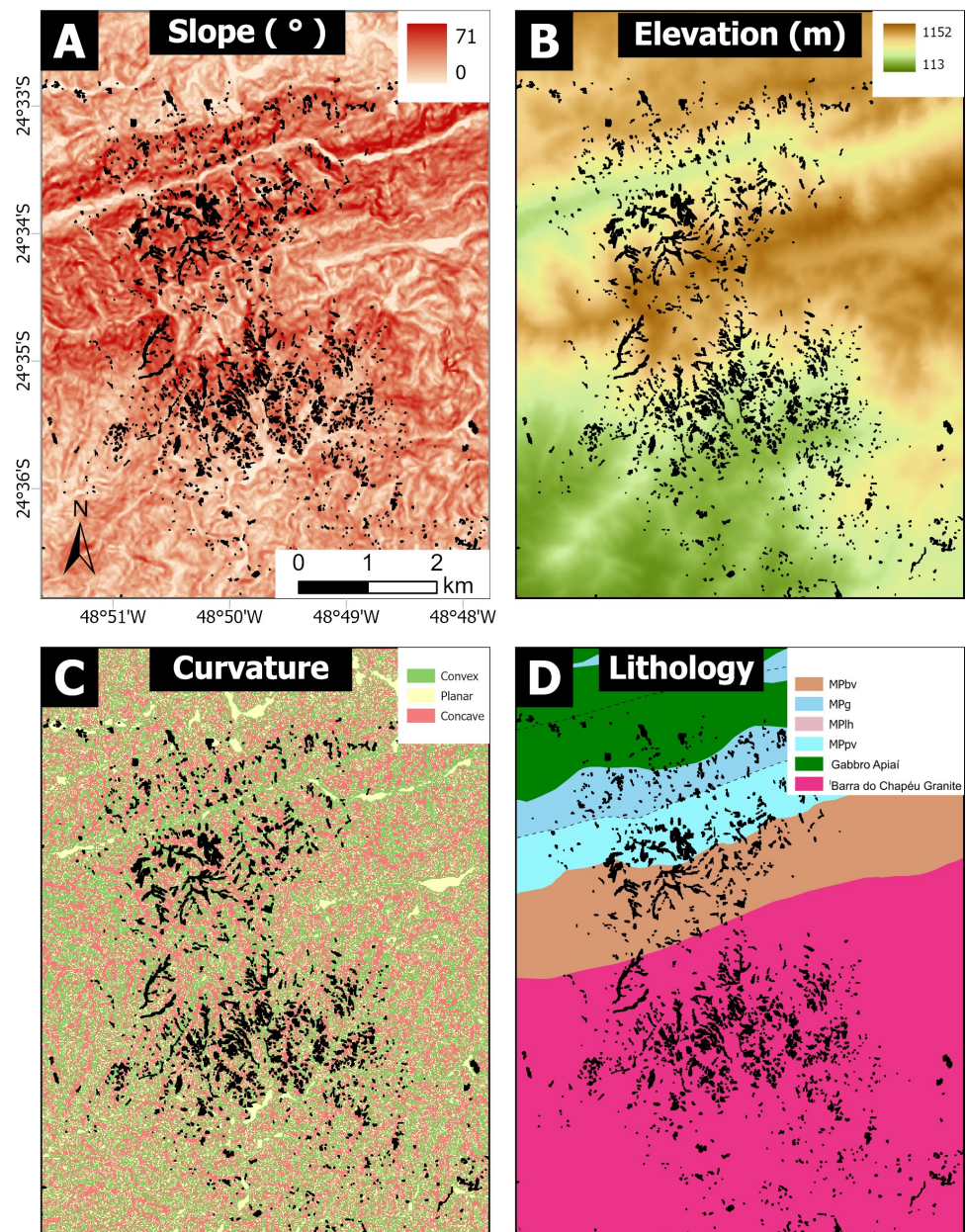| Spectral	NDVI	High Frequency: 0.1–0.32; Min: −0.16/Max: 0.32
	Slope degree	High frequency: 15–30°; Min: 5.6°/Max: 59.8°
Morphology	Elevation	High frequency: 300–600 m; Min: 158.1/Max: 968.9 m
	Curvature	High frequency: −0.2–0.1; Min: −4.5/Max: 5.3

Figure 5. Shallow landslides (black features), morphological and lithological characteristics of Itaóca: (**A**) slope; (**B**) elevation; (**C**) curvature; and (**D**) lithology.

Table 4. Spatial accuracy metrics calculated for two different patterns of shallow landslide scars: large and elongated (north); small-to-medium and rounded (central and south).

Spatial Accuracy Metrics	Northern Sector	Central and Southern Sector
QR	0.52	0.59
AFI	0.23	0.20
OS	0.43	0.48
US	0.25	0.35
D	0.35	0.42

4.2. Rule Set Transferability

The semi-automated object-based classification of shallow landslides for Nova Friburgo is presented in Figure 6. In general, the OBIA classification overestimates the reference. A total area of 11.38 km^2 was identified as shallow landslides through the OBIA classification,

while the reference mapping indicated an area of 6.42 km^2. The Nova Friburgo OBIA inventory presents a higher number of false positives than the Itaóca inventory. Despite the overestimation, our results are promising and indicate the good transferability of the OBIA method in Brazil. In Itaóca, shallow landslides of various sizes occurred, whereas in Nova Friburgo, large landslides were more common. In Itaóca, the mean size was 1900 m^2 with a median of 725 m^2, while in Nova Friburgo, the mean size was 3200 m^2 with a median of 725 m^2. The rule set utilized for both study sites consisted of identical classification features and parameters, albeit with slight adjustments in thresholds. For instance, the mean NDVI and slope values were tailored to align with the specific environmental and geomorphological conditions in each locality. The outcomes affirm the method's applicability in Brazil, although additional modifications to the primary rule set might lead to better results.
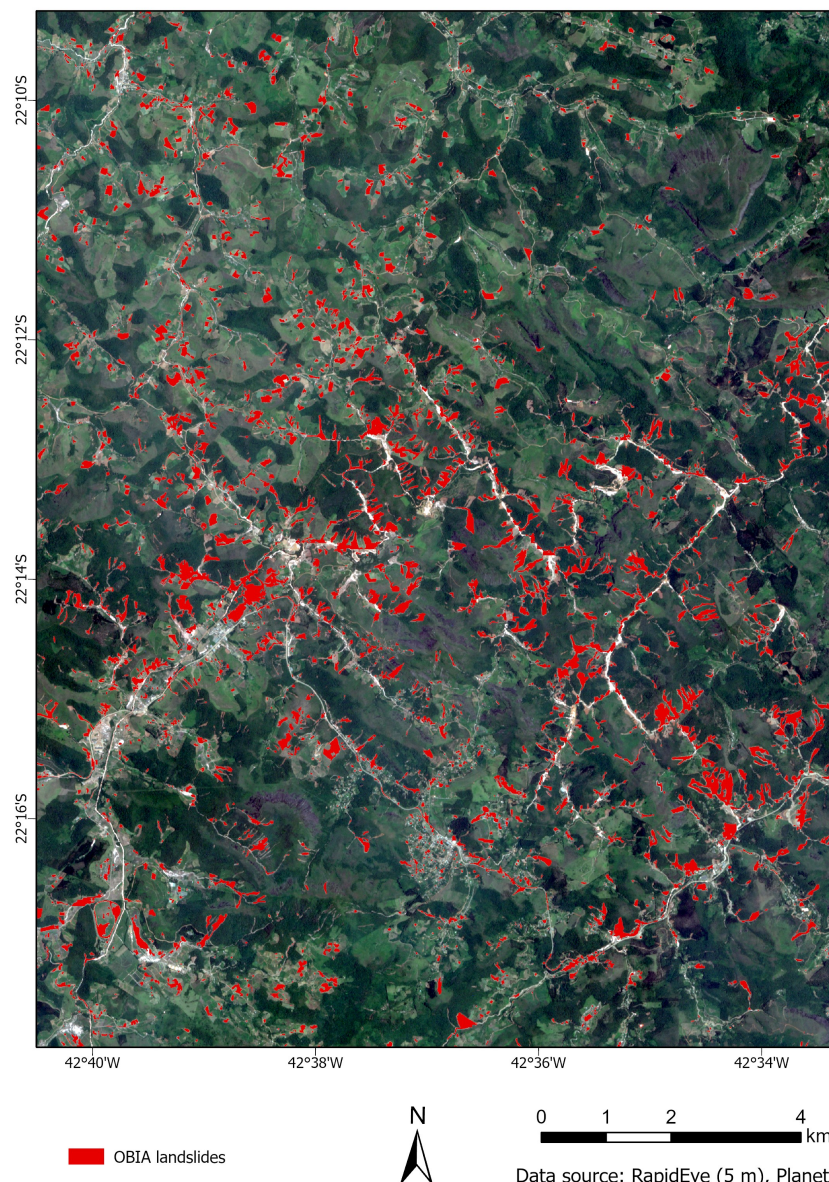

Figure 6. Shallow landslide mapping result in Nova Friburgo (RJ) using OBIA.

4.3. Common Classification Errors

The object-based method demonstrated its suitability for identifying shallow landslides in Brazil. Nonetheless, some errors occurred, whereby most of them are characterized as *FP*, defined as objects that were wrongly classified (Figures 7 and 8). The *FP* identified in Itaóca and Nova Friburgo varied because of specific local characteristics. In Itaóca, the

primary *FP* errors were associated with non-vegetated areas, and there were instances where debris flows were incorrectly classified as shallow landslides (Figure 7). In Nova Friburgo, the main *FPs* were non-vegetated areas and urban infrastructure such as roads and built-up areas (Figure 8). The *FN* objects in both study sites were mainly small features and scar delineation.
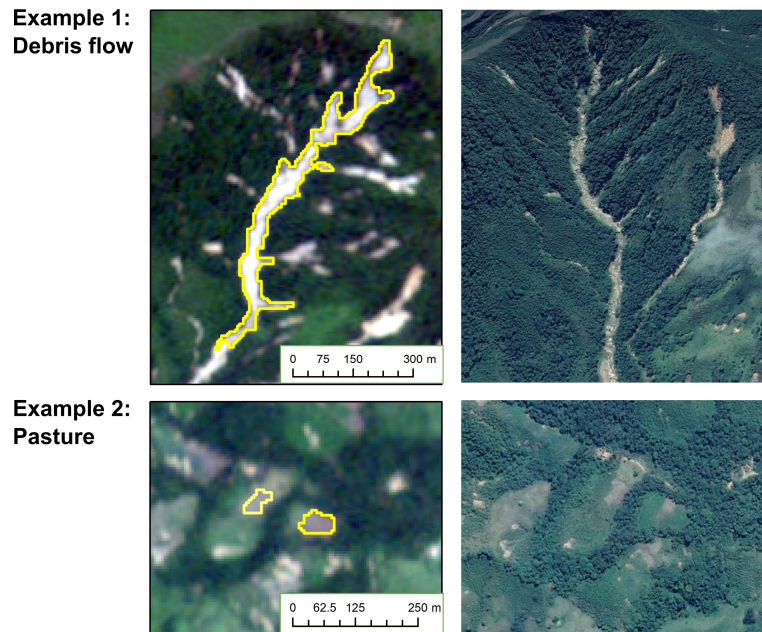

Figure 7. Common classification errors in Itaóca (SP): non-vegetated areas and debris flows. RapidEye (**left**) and Google Earth images (**right**) were used for comparison.

Figure 8. Common classification errors in Nova Friburgo (RJ): non-vegetated areas and urban infrastructure. RapidEye (**left**) and Google Earth images (**right**) were used for comparison.

5. Discussion

Rainfall-induced landslide inventories are commonly constructed worldwide based on a variety of methods [15,18,19,32,63,64]. The semi-automated object-based classification correctly identified most locations with shallow landslides, but some errors were identified. Schwarz et al. [20] investigated the different effects of manual and semi-automatic inventory mapping on the landslide morphological characteristics in Rio Grande do Sul, Brazil. They used a semi-automated method based on the Modified Soil Adjusted Vegetation Index 2 (MSAVI2) variation, adopting a minimum slope threshold. The authors highlighted the differences in the number of landslides in each inventory owing to the tendency of grouping landslides in the semi-automatic method, a behavior was also identified in our OBIA inventory. The OBIA method has its limitations; it can miss some small features, and erroneously merge neighboring features into larger polygons [30]. The spatial overlap of the detected landslides and reference mapping was 54%. Similar findings in a tropical environment were reported by Schwarz et al. [20] and Hölbling et al. [22] in Italy. The notable disparities in the total number of features when comparing the OBIA and the reference dataset primarily stem from the fact that some small shallow landslide features were not recognized with OBIA (Figure 3E); similar obstacles were identified in southeastern Brazil [15,65]. The primary limitation lies in the fact that the available data resolution in the study area did not allow for the complete identification of small shallow landslide scars. These findings can be attributed to several factors. The semi-automated detection of shallow landslides with OBIA relies on spectral, spatial, and morphological differences between the landslides and surrounding features. OBIA performs effectively in identifying landslide source areas but exhibits reduced accuracy in recognizing landslide tails and delineating scars, as well as in detecting small landslide features. This can likely be explained by the limited resolution of the RapidEye data (5 m), as well as the absence of discernible spectral, spatial, or morphological attributes that could have been employed during semi-automated mapping for the recognition of tails [62] and small landslide features. Several small landslides were missed by OBIA, thus, the correct detection of small scars requires expert knowledge. Such expert skills can hardly be directly transferred into classification rule sets and remain a challenge [26,62], and only a few attempts have been made to objectivize the classification step by integrating common expert knowledge [66]. While further steps in this direction are needed, we attempted to keep the classification rule set as simple as possible and applied commonly used classification features to increase the transferability, comprehensibility, and replicability. Nevertheless, large shallow landslides were well recognized by the OBIA approach (Figure 3C). The accuracy metrics yielded results above 79% that were consistent with those reported in the existing literature, [15,18,29,30]. All the spatial accuracy indexes were below 0.55, indicating a good-to-high agreement between the manual and the semi-automated classification. However, accuracy numbers should be treated with care, since most manually prepared reference data, despite often being the best available reference, also include uncertainties due to the data used, the skills of the interpreter, and study area characteristics [23]. Nevertheless, we believe that the reference data used are of high quality, as confirmed by visual checks.

The distinct landslide shape patterns identified in the study site in Itaóca can be explained by the lithology (Figure 5D). The northern sector consists of the Lajeado metasedimentary group (metamorphic rocks: marble, phyllite, schist, and quartzite), and the central and southern sectors are constituted by the Itaóca batholith zone (igneous rocks: granites). The morphology of the landscape is influenced by the rock weathering profile, which develops through mechanical or chemical weathering processes. This profile can vary significantly from one location to another due to local differences in rock type, geological structure, topography, erosion rates, groundwater conditions, and climate variations, as noted by Gerrard [67]. The scars in the Lajeado metasedimentary group tend to develop a longer and larger shape because they are conditioned by structural weakness planes in rocks (e.g., sedimentary layers, granulometric difference, metamorphic banding). Granite

scars, on the other hand, tend to develop a rounded shape as they depend more on joint networks which in turn affect the process of weathering and soil formation [67,68]. The relevance of the role of lithology in the recognition of shallow landslides using remote sensing methods is clearly supported by the current findings. Regarding the morphological characteristics of each scar shape type, the negative values for plan curvature are similar, but the slope angle and elevation vary. A negative curvature value indicates that the surface prior to the event was concave, which makes it responsible for the convergence of materials and flows, as described in previous studies [69–71]. Long and large scars are more frequent between 21 and 40° and 500–870 m. However, small to medium and rounded scars are common between 10 and 30° and 300–600 m. These results suggest that a combination of slope, elevation, curvature, and lithology can indeed impact the location and morphology of shallow landslide scars.

Regarding the transferability of the approach, the semi-automated object-based classification of shallow landslides for Nova Friburgo overestimates the reference. Hölbling et al. [23] also encountered similar challenges and confirmed that the transferability is contingent upon the specific characteristics of satellite images, the study areas in question, and the complexity and visual characteristics of shallow landslides. Despite the overestimation, our results are promising and indicate the good transferability of the OBIA method in Brazil. *FP* and *FN* classification errors were identified in Itaóca and Nova Friburgo. These findings align with those observed in other remote sensing-based landslide mapping studies conducted in Brazil [15,18] and worldwide [22,62]. These studies mentioned similar challenges in landslide detection, as we experienced in this study.

Rainfall-induced landslide inventories are crucial for local stakeholders and decision makers. Having information about the spatial distribution of these hazards is essential for effective disaster management, especially in the context of climate change. According to Alves et al. [72], the erosive power of rainfall is directly affected by climate change, which, in turn, impacts the vulnerability of mountainous environments to natural hazards like landslides. The study conducted by Alves et al. [72] in the state of Rio de Janeiro raised concerns about the potential occurrence of extreme rainfall-related disasters in the near future.

6. Conclusions

An object-based approach was employed for the classification of shallow landslides in Itaóca (Brazil). Spatial, spectral, and morphological data were utilized for the segmentation and subsequent classification of objects, all based on a high-resolution satellite image. The results suggest that the OBIA method is well suited for application in the tropical environments of Brazil. The approach correctly identified locations with shallow landslides, but the semi-automated classification underestimated the reference, with a deviation of approximately 21%. Two distinct patterns of landslide shapes were visually identified, leading us to conclude that lithology can impact the morphology of shallow landslide scars. This, in turn, can affect the recognition and accuracy of landslide features when utilizing remote sensing approaches and data. The main challenges were the identification of small scars, landslide tails, and scar delineation. This can likely be explained by the limited resolution of the RapidEye data (5 m). Regarding transferability, the Nova Friburgo OBIA inventory presents a higher number of false positives in comparison to Itaóca, because Nova Friburgo presents a more complex environment. The rule set applied in Itaóca and Nova Friburgo included the same classification features and parameters but with slightly modified thresholds. The findings affirm the potential for transferring the approach to different regions in Brazil. However, it is worth noting that further adjustments to the primary rule set could potentially yield improved results. Further improvements could be made with higher-resolution EO data in future studies. This could lead to an enhanced mapping accuracy and help mitigate common classification errors. The results can prove valuable for local stakeholders and decision makers, as having information about

the location and spatial distribution of shallow landslides is crucial for effective disaster management and territorial planning.

References

1. CRED. *Disasters in Numbers 2021*; Technical Report; Centre for Research on the Epidemiology of Disasters: Brussels, Belgium , 2022.
2. Alcántara-Ayala, I. Time in a bottle: Challenges to disaster studies in Latin America and the Caribbean. *Disasters* **2019**, *43*, 18–27. [CrossRef] [PubMed]
3. Coelho-Netto, A.L.; de Souza Avelar, A.; Lacerda, W.A. Landslides and Disasters in Southeastern and Southern Brazil. In *Natural Hazards and Human-Exacerbated Disasters in Latin America*; Elsevier: Amsterdam, The Netherlands, 2009; pp. 223–243. [CrossRef]
4. Vieira, B.C.; Gramani, M.F., Serra do Mar: The most tormented relief in Brazil. In *Landscapes and Landforms of Brazil*; Springer: Dordrecht, The Netherlands, 2015; pp. 285–297.
5. IBGE. *Suscetibilidade a Deslizamentos do Brasil: Primeira Aproximação*; Technical Report; Instituto Brasileiro de Geografia e Estatística: Rio de Janeiro, Brazil, 2019.
6. Alvalá, R.C.D.S.; Assis Dias, M.C.; Saito, S.M.; Stenner, C.; Franco, C.; Amadeu, P.; Ribeiro, J.; Santana, R.A.S.M.; Nobre, C.A. Mapping characteristics of at-risk population to disasters in the context of Brazilian early warning system. *Int. J. Disaster Risk Reduct.* **2019**, *41*, 101326. [CrossRef]
7. Saito, S.M.; de Assis Dias, M.C.; Ribeiro, D.F.; dos Santos Alvalá, R.C.; de Souza, D.B.; de Moraes Santana, R.A.S.; de Souza, P.A.; Ribeiro, J.V.M.; Stenner, C. Disaster risk areas in Brazil: Outcomes from an intra-urban scale analysis. *Int. J. Disaster Resil. Built Environ.* **2021**, *12*, 238–250. [CrossRef]
8. Dias, H.C.; Hölbling, D.; Grohmann, C.H. Landslide Inventory Mapping in Brazil: Status and challenges. In Proceedings of the XIII International Symposium on Landslides, Cartagena, Colombia, 22–26 February 2021.
9. Dias, H.C.; Hölbling, D.; Grohmann, C.H. Landslide Susceptibility Mapping in Brazil: A Review. *Geosciences* **2021**, *11*, 425. [CrossRef]
10. Guzzetti, F.; Cardinali, M.; Reichenbach, P.; Carrara, A. Comparing Landslide Maps: A Case Study in the Upper Tiber River Basin, Central Italy. *Environ. Manag.* **2000**, *25*, 247–263. [CrossRef]
11. Avelar, A.S.; Netto, A.L.C.; Lacerda, W.A.; Becker, L.B.; Mendonça, M.B. Mechanisms of the Recent Catastrophic Landslides in the Mountainous Range of Rio de Janeiro, Brazil. In *Landslide Science and Practice*; Springer: Berlin/Heidelberg, Germany, 2013; pp. 265–270. [CrossRef]
12. Netto, A.L.C.; Sato, A.M.; de Souza Avelar, A.; Vianna, L.G.G.; Araújo, I.S.; Ferreira, D.L.C.; Lima, P.H.; Silva, A.P.A.; Silva, R.P. January 2011: The Extreme Landslide Disaster in Brazil. In *Landslide Science and Practice*; Springer: Berlin/Heidelberg, Germany, 2013; pp. 377–384. [CrossRef]
13. Carou, C.B.; Vieira, B.C.; Martins, T.D.; Gramani, M.F. Inventário dos escorregamentos da Bacia do rio Gurutuba, Vale do Ribeira (SP). *Rev. Dep. Geogr.* **2017**, 172–179. [CrossRef]
14. Dias, H.C.; Hölbling, D.; Grohmann, C.H. Shallow landslide mapping using freely accessible images: A case study in the Ribeira Valley, Brazil. In Proceedings of the EGU General Assembly 2021, Online, 19–30 April 2021. . [CrossRef]
15. Dias, H.C.; Sandre, L.H.; Alarcón, D.A.S.; Grohmann, C.H.; Quintanilha, J.A. Landslide recognition using SVM, Random Forest, and Maximum Likelihood classifiers on high-resolution satellite images: A case study of Itaóca, southeastern Brazil. *Braz. J. Geol.* **2021**, *51*, e20200105. [CrossRef]
16. da Silva, D.F.S.; Corteletti, R.C.; Filgueiras, R.A.C.; Santos, A.E.M. Correlations between landslide scars parameters using remote sensing methods in the estrada de ferro Vitória-Minas, southeastern Brazil. *Rev. Bras. Geomorfol.* **2021**, *22*, 297–314. [CrossRef]

17. Uehara, T.D.T.; Körting, T.S.; dos Reis Soares, A.; Quevedo, R.P. Time-series metrics applied to land use and land cover mapping with focus on landslide detection. *J. Appl. Remote Sens.* **2022**, *16*, 034518. [CrossRef]

18. Soares, L.P.; Dias, H.C.; Garcia, G.P.B.; Grohmann, C.H. Landslide Segmentation with Deep Learning: Evaluating Model Generalization in Rainfall-Induced Landslides in Brazil. *Remote Sens.* **2022**, *14*, 2237. [CrossRef]

19. Xu, G.; Wang, Y.; Wang, L.; Soares, L.P.; Grohmann, C.H. Feature-Based Constraint Deep CNN Method for Mapping Rainfall-Induced Landslides in Remote Regions With Mountainous Terrain: An Application to Brazil. *IEEE J. Sel. Top. Appl. Earth Obs. Remote Sens.* **2022**, *15*, 2644–2659. [CrossRef]

20. Schwarz, H.; Michel, G.P.; Zanandrea, F.; Paul, L.R.; Salvador, C.G. Uso de caracterização morfométrica e geomorfológica na análise de mapeamentos de cicatrizes de escorregamentos. *Rev. Bras. Geomorfol.* **2023**, *24*, e2185. [CrossRef]

21. Martha, T.R.; Kerle, N.; Jetten, V.; van Westen, C.J.; Kumar, K.V. Characterising spectral, spatial and morphometric properties of landslides for semi-automatic detection using object-oriented methods. *Geomorphology* **2010**, *116*, 24–36. [CrossRef]

22. Hölbling, D.; Füreder, P.; Antolini, F.; Cigna, F.; Casagli, N.; Lang, S. A Semi-Automated Object-Based Approach for Landslide Detection Validated by Persistent Scatterer Interferometry Measures and Landslide Inventories. *Remote Sens.* **2012**, *4*, 1310–1336. [CrossRef]

23. Hölbling, D.; Eisank, C.; Albrecht, F.; Vecchiotti, F.; Friedl, B.; Weinke, E.; Kociu, A. Comparing Manual and Semi-Automated Landslide Mapping Based on Optical Satellite Images from Different Sensors. *Geosciences* **2017**, *7*, 37. [CrossRef]

24. Comert, R.; Avdan, U.; Gorum, T.; Nefeslioglu, H.A. Mapping of shallow landslides with object-based image analysis from unmanned aerial vehicle data. *Eng. Geol.* **2019**, *260*, 105264. [CrossRef]

25. Karantanellis, E.; Marinos, V.; Vassilakis, E.; Hölbling, D. Evaluation of Machine Learning Algorithms for Object-Based Mapping of Landslide Zones Using UAV Data. *Geosciences* **2021**, *11*, 305. [CrossRef]

26. Hölbling, D. Data and knowledge integration for object-based landslide mapping—Challenges, opportunities and applications. *gis. Sci. Z. Geoinform.* **2022**, *1*, 1–13.

27. Stumpf, A.; Kerle, N. Object-oriented mapping of landslides using Random Forests. *Remote Sens. Environ.* **2011**, *115*, 2564–2577. [CrossRef]

28. Heleno, S.; Matias, M.; Pina, P.; Sousa, A.J. Semiautomated object-based classification of rain-induced landslides with VHR multispectral images on Madeira Island. *Nat. Hazards Earth Syst. Sci.* **2016**, *16*, 1035–1048. [CrossRef]

29. Hölbling, D.; Friedl, B.; Eisank, C. An object-based approach for semi-automated landslide change detection and attribution of changes to landslide classes in northern Taiwan. *Earth Sci. Inform.* **2015**, *8*, 327–335. [CrossRef]

30. Dias, H.C.; Hölbling, D.; Dias, V.C.; Grohmann, C.H. Application of Object-Based Image Analysis for Detecting and Differentiating between Shallow Landslides and Debris Flows. *GI Forum* **2023**, *1*, 34–44. [CrossRef]

31. Knevels, R.; Petschko, H.; Leopold, P.; Brenning, A. Geographic Object-Based Image Analysis for Automated Landslide Detection Using Open Source GIS Software. *ISPRS Int. J. Geo-Inf.* **2019**, *8*, 551. [CrossRef]

32. Amatya, P.; Kirschbaum, D.; Stanley, T.; Tanyas, H. Landslide mapping using object-based image analysis and open source tools. *Eng. Geol.* **2021**, *282*, 106000. [CrossRef]

33. Hölbling, D.; Abad, L.; Dabiri, Z.; Prasicek, G.; Tsai, T.T.; Argentin, A.L. Mapping and Analyzing the Evolution of the Butangbunasi Landslide Using Landsat Time Series with Respect to Heavy Rainfall Events during Typhoons. *Appl. Sci.* **2020**, *10*, 630. [CrossRef]

34. Machado, C.A.S.; Quintanilha, J.A. Identification of trip generators using remote sensing and geographic information system. *Transp. Res. Interdiscip. Perspect.* **2019**, *3*, 100069. [CrossRef]

35. Manfré, L.A.; Cruz, B.B.; Quintanilha, J.A. Urban Settlements and Road Network Analysis on the Surrounding Area of the Almirante Alvaro Alberto Nuclear Complex, Angra dos Reis, Brazil. *Appl. Spat. Anal. Policy* **2020**, *13*, 209–221. [CrossRef]

36. Utsumi, A.G.; Pissarra, T.C.T.; Rosalen, D.L.; Filho, M.V.M.; Rotta, L.H.S. Gully mapping using geographic object-based image analysis: A case study at catchment scale in the Brazilian Cerrado. *Remote Sens. Appl. Soc. Environ.* **2020**, *20*, 100399. [CrossRef]

37. Zoffoli, M.L.; Frouin, R.; Moura, R.L.; de Medeiros, T.A.G.; Bastos, A.C.; Kampel, M. Spatial distribution patterns of coral reefs in the Abrolhos region (Brazil, South Atlantic ocean). *Cont. Shelf Res.* **2022**, *246*, 104808. [CrossRef]

38. de Medeiros, T.P.; Morellato, L.P.C.; Silva, T.S.F. Spatial distribution and temporal variation of tropical mountaintop vegetation through images obtained by drones. *Front. Environ. Sci.* **2023**, *11*, 1083328. [CrossRef]

39. Blaschke, T. Object based image analysis for remote sensing. *ISPRS J. Photogramm. Remote Sens.* **2010**, *65*, 2–16. [CrossRef]

40. Lillesand, T.; Kiefer, R.W.; Chipman, J. *Remote Sensing and Image Interpretation*; John Wiley & Sons: Hoboken, NJ, USA, 2015.

41. Hossain, M.D.; Chen, D. Segmentation for Object-Based Image Analysis (OBIA): A review of algorithms and challenges from remote sensing perspective. *ISPRS J. Photogramm. Remote Sens.* **2019**, *150*, 115–134. . [CrossRef]

42. Su, T.; Zhang, S. Local and global evaluation for remote sensing image segmentation. *ISPRS J. Photogramm. Remote Sens.* **2017**, *130*, 256–276. [CrossRef]

43. Guzzetti, F.; Mondini, A.C.; Cardinali, M.; Fiorucci, F.; Santangelo, M.; Chang, K.T. Landslide inventory maps: New tools for an old problem. *Earth-Sci. Rev.* **2012**, *112*, 42–66. [CrossRef]

44. IBGE. *Censo Demográfico 2010*; Technical Report; Instituto Brasileiro de Geografia e Estatística: Rio de Janeiro, Brazil, 2010.

45. Ross, J.L.S. A morfogênese da bacia do Ribeira do Iguape e os sistemas ambientais. *GEOUSP Espaç. Tempo* **2002**, *6*, 21–46.

46. Faleiros, F.; Morais, S.; Costa, V. *Geologia dos Recursos Naturais da Folha Apiaí- SG.22-X-B-V, Estados de São Paulo e Paraná—Escala 1:100.000*; Technical Report; CPRM: São Paulo, Brazil, 2012; 107p.
47. Zenero, J.; Vieira, O.; Godoy, A. Geologia e Litogeoquímica do Batólito de Itaóca, Sul do estado de São Paulo. *Geociências* **2020**, *39*, 317–342. . [CrossRef]
48. Rossi, M. *Mapa Pedológico do Estado de São Paulo: Revisado e Ampliado*; Instituto Florestal: São Paulo, Brazil, 2017; Volume 1, p. 118.
49. Brollo, M.J.; Santoro, J.; Penteado, D.R.; da Silva, P.C.F.; Ribeiro, R.R. Itaóca (SP): Histórico de acidentes e desastres relacionados a perigos geológicos. In Proceedings of the XIV Simpósio de Geologia do Sudeste, Campos do Jordão, Brazil, 26–29 October 2015.
50. Gramani, M.; Martins, V. Debris flows occurrence by intense rains at Itaoca city, São Paulo, Brazil: Field observations. In *Landslides and Engineered Slopes: Experience, Theory and Practice*; CRC Press: Boca Raton, FL, USA, 2016; pp. 1011–1019.
51. Dias, V.C.; McDougall, S.; Vieira, B.C. Geomorphic analyses of two recent debris flows in Brazil. *J. S. Am. Earth Sci.* **2022**, *113*, 103675. [CrossRef]
52. Dantas, M.E. *Geomorfologia do Estado do Rio de Janeiro: Estudo Geoambiental do Estado do Rio de Janeiro*; CPRM: Brasília, Brazil, 2001.
53. Tupinambá, M.; Heilbron, M.; Duarte, B.P.; de Almeida, J.C.H.; Valladares, C.S.; Pacheco, B.T.; dos Santos Salomão, M.; Conceição, F.R.; da Silva, L.G.E.; de Almeida, C.G.; et al. *Mapa Geológico Folha Nova Friburgo SF-23-Z-B-II*; Technical Report; CPRM—Serviço Geológico do Brasil: Belo Horizonte, Brazil, 2012.
54. Planet. *Planet Imagery Products Specifications*; Planet Labs: San Francisco, CA, USA, 2022.
55. Bhandari, A.K.; Kumar, A.; Singh, G.K. Feature Extraction using Normalized Difference Vegetation Index (NDVI): A Case Study of Jabalpur City. *Procedia Technol.* **2012**, *6*, 612–621. [CrossRef]
56. Uehara, T.D.T.; Corrêa, S.P.L.P.; Quevedo, R.P.; Körting, T.S.; Dutra, L.V.; Rennó, C.D. Landslide Scars Detection using Remote Sensing and Pattern Recognition Techniques: Comparison among Artificial Neural Networks, Gaussian Maximum Likelihood, Random Forest, and Support Vector Machine Classifiers. *Rev. Bras. Cartogr.* **2020**, *72*, 665–680. [CrossRef]
57. DAAC, A. *ALOS PALSAR Radiometric Terrain Corrected High Res; Includes Material JAXA/METI 2011*; Technical Report; Alaska Satellite Facility: Fairbanks, AK, USA, 2020.
58. Benz, U.C.; Hofmann, P.; Willhauck, G.; Lingenfelder, I.; Heynen, M. Multi-resolution, object-oriented fuzzy analysis of remote sensing data for GIS-ready information. *PRS J. Photogramm. Remote Sens.* **2004**, *58*, 239–258. [CrossRef]
59. Rosenfield, G.; Fitzptrik-Lins, K.; Ling, S. Sampling for thematicmap accuracy testing. *Photogramm. Eng. Remote Sens.* **1982**, *48*, 131–137.
60. Congalton, R.G. A review of assessing the accuracy of classifications of remotely sensed data. *Remote Sens. Environ.* **1991**, *37*, 35–46. [CrossRef]
61. Eisank, C.; Smith, M.; Hillier, J. Assessment of multiresolution segmentation for delimiting drumlins in digital elevation models. *Geomorphology* **2014**, *214*, 452–464. [CrossRef] [PubMed]
62. Hölbling, D.; Betts, H.; Spiekermann, R.; Phillips, C. Identifying Spatio-Temporal Landslide Hotspots on North Island, New Zealand, by Analyzing Historical and Recent Aerial Photography. *Geosciences* **2016**, *6*, 48. [CrossRef]
63. Peruccacci, S.; Gariano, S.L.; Melillo, M.; Solimano, M.; Guzzetti, F.; Brunetti, M.T. The ITAlian rainfall-induced LandslIdes CAtalogue, an extensive and accurate spatio-temporal catalogue of rainfall-induced landslides in Italy. *Earth Syst. Sci. Data* **2023**, *15*, 2863–2877. [CrossRef]
64. Garcia, G.P.B.; Soares, L.P.; Espadoto, M.; Grohmann, C.H. Relict landslide detection using deep-learning architectures for image segmentation in rainforest areas: A new framework. *Int. J. Remote Sens.* **2023**, *44*, 2168–2195. [CrossRef]
65. Marcelino, E.V.; Formaggio, A.R.; Maeda, E.E. Landslide inventory using image fusion techniques in Brazil. *Int. J. Appl. Earth Obs. Geoinf.* **2009**, *11*, 181–191. [CrossRef]
66. Eisank, C.; Hölbling, D.; Friedl, B.; Chen, Y.C.; Chang, K.T. Expert knowledge for object-based landslide mapping in Taiwan. *South-East. Eur. J. Earth Obs. Geomat.* **2014**, *3*, 347–350.
67. Gerrard, A.J. *Rocks and Landforms*; Springer: Dordrecht, The Netherlands, 1988. [CrossRef]
68. Lin, C.C.; Gramani, M.F.; de Campos, A.B. Levantamento das cicatrizes de deslizamentos na bacia do Rio Gurutuba (SP) e correlações com parâmetros físicos. In Proceedings of the XVIII Congresso Brasileiro de Mecânica dos Solos e Engenharia Geotécnica, Belo Horizonte, Brazil, 19–22 October 2016.
69. Fernandes, N.F.; Guimarães, R.F.; Gomes, R.A.T.; Vieira, B.C.; Montgomery, D.R.; Greenberg, H. Condicionantes Geomorfológicos dos Deslizamentos nas Encostas: Avaliação de Metodologias e Aplicação de Modelo de Previsão de Áreas Susceptíveis. *Rev. Bras. Geomorfol.* **2001**, *2*, 51–71. [CrossRef]
70. Dias, H.C.; Dias, V.C.; Vieira, B.C. Condicionantes Morfológicos e Geológicos dos Escorregamentos Rasos na Bacia do Rio Santo Antônio, Caraguatatuba/SP. *Rev. Dep. Geogr.* **2017**, 157–163. [CrossRef]
71. Martins, T.D.; Oka-Fiori, C.; Vieira, B.C.; de Barros Correa, A.C.; Bateira, C.V.M. Análise dos parâmetros morfológicos de escorregamentos rasos na Serra do Mar, Paraná. *Caminhos Geogr.* **2017**, *18*, 223–239. [CrossRef]
72. Alves, G.J.; Mello, C.R.; Guo, L. Rainfall disasters under the changing climate: A case study for the Rio de Janeiro mountainous region. *Nat. Hazards* **2023**, *116*, 1539–1556. [CrossRef]